Colloid and Interface Science Communications 35 (2020) 100235

Contents lists available at ScienceDirect

Colloid and Interface Science Communications

journal homepage: www.elsevier.com/locate/colcom

CD44 receptor targeted 'smart' multi-walled carbon nanotubes for synergistic therapy of triple-negative breast cancer

Nidhi Jain Singhai[a], Rahul Maheshwari[b], Suman Ramteke[a,*]

[a] School of Pharmaceutical Sciences, Rajiv Gandhi Proudyogiki Vishwavidyalaya, Bhopal 462033, MP, India
[b] School of Pharmacy and Technology Management, SVKM's NMIMS, Hyderabad, Telangana 509 301, India

ARTICLE INFO

Keywords:
Targeted chemotherapy
Multi-walled carbon nanotubes
Hyaluronic acid
α-Tocopheryl succinate
Doxorubicin
Synergistic anticancer therapy

ABSTRACT

Triple-negative breast cancer requires high treatment specificity and efficacy due to its aggressive nature. In the present investigation, multi-walled carbon-nanotubes (MWCNTs) were functionalized using Hyaluronic acid (HA) and α-Tocopheryl succinate (α-TOS) and loaded with Doxorubicin (Dox) to obtained novel α-TOS-HA-MWCNTs/Dox conjugate to achieve enhanced cellular-placement and anticancer-therapeutic action against CD44 receptors overexpressing TNBC cells (MDA-MB-231). Interestingly, α-TOS-HA-MWCNTs/Dox displayed high cellular uptake as compared to individually tailored MWCNTs formulations. Anticancer investigation revealed prominent growth inhibition effect (SRB assay; GI_{50}; 0.810 ± 0.017; $p < .001$) and high total apoptotic ratio (Annexin V/PI assay; 52.69 ± 4.86%; $p < .005$) in the MDA-MB-231 cells treated using α-TOS-HA-MWCNTs/Dox as compared to other formulations. Findings suggest that HA and α-TOS could be employed as a synergistic, safe, and effective **tumor**-targeted chemotherapy.

1. Introduction

Triple-negative breast cancer (TNBC), lacks the presence of estrogen, progesterone, and human epidermal growth factor-2 (HER-2) receptors and therefore very challenging to diagnose and treat [1,2]. Besides, the low frequency of TNBC driven by rare aberrations imposed limitations for ad hoc drug development and lack of specific marker of the TNBC is another big challenge to design formulation strategy. TNBC treatment involves chemotherapy and radiation therapy, which suffers from severe drawbacks such as multidrug resistance, cytotoxicity, and tissue damage. Hormonal therapeutics is not recommended treatment for TNBC due to the loss of target receptors. Till date, surgery and chemotherapy, individually or in combination, are the only available treatment for TNBC [3,4].

Moreover, the majority of chemo-specific molecules fails to attain effective therapeutic concentration without harming the normal cells [5], due to their nonselective tumor accumulation [6]. Effective and safe treatment of TNBC requires the maximum exposure of therapeutic molecules to cancerous tissues/cells while minimum reachability to non-cancerous cells, and that could be achieved by selecting an appropriate targeted drug delivery system [7–9].

Nanotechnology-based approaches for delivering therapeutic cargo could serve as an effective strategy to overcome most of the adverse effects resulting from the use of conventional chemotherapy practice [10,11]. Reports are available suggesting that nanotechnology-based designer delivery systems such as dendrimers, liposomes, polymeric nanoparticles, and carbonaceous materials have improved anticancer efficacy and redefined the way of delivering the drugs to the cancer sites by imparting a high level of specificity [12–14]. Among them, multi-walled carbon nanotubes (MWCNTs) have gained wide attention in engaging the therapeutic molecules for effective and potential treatment of various cancers including breast, lung and liver cancer owing to their excellent physicochemical properties [15]. Our selection of MWCNTs over SWCNTs was due to high drug entrapment efficiency inside the cone and inner walls of MWCNTs along with minimum drug leakage over time and excellent mechanical strength than that of SWCNTs. Besides, large scale production of MWCNTs is much cheaper than that of SWCNTs [15–17]. Recently, Arkan et al., employed gold nanoparticles modified MWCNTs to fabricate novel immunosensor for the detection of HER2 in serum samples as a lead in breast cancer treatment [18]. Similarly, Prajapati et al., evaluated in vitro and in vivo potential of gemcitabine (GEM) loaded hyaluronic acid (HA) conjugated multi-walled carbon nanotubes (GEM/HA- PEG-MWCNTs) for effective colon cancer targeting [19]. However, to obtain targeted/site-specific delivery, accurate placement and accumulation of drug molecule are required in the cancer cells, which can be made possible by increasing the cellular uptake of the drug via employing suitable targeting ligand.

* Corresponding author.
E-mail address: sapna1731@rediffmail.com (S. Ramteke).

https://doi.org/10.1016/j.colcom.2020.100235
Received 2 December 2019; Received in revised form 11 January 2020; Accepted 15 January 2020

In the past couple of years, Hyaluronic acid (HA), as naturally occurring carbohydrate (glycosaminoglycan) based multiunit chain of d-glucuronic acid and glucosamine, has been widely explored as targeting tool owing to its high specificity towards CD44 receptors over-expressing cancer cells [20–22]. As a fact, CD44 receptors are highly expressed on the surface of a variety of cancer cells and reported to plays a very crucial role in cellular responses such as cellular proliferation, migration, and invasion [23–25]. Another aspect of using HA as targeting ligand is the availability of functional groups on its surface that could be engineered to form specific conjugates for particular applications [26]. Yao et al. recently developed SWCNTs as drug delivery platforms and achieved higher intracellular epirubicin concentration to overcome multidrug resistance in A549/Taxol cells [27]. Similarly, Cao et al., fabricated MWCNTs functionalized using HA for the treatment of breast cancer [28]. However, the synergistic anti-cancer therapy is the need of the hour and addition of specific molecules that provoke the anti-cancer effect in cancer cells while un-affecting the healthy cells is more promising.

In context, α-Tocopheryl succinate (α-TOS; vitamin E succinate) which is a succinyl derivative of vitamin E, well-known for its anti-cancer properties mainly via an apoptotic pathway and at the same time reported being non-toxic to healthy cells [29]. This property makes α-TOS particularly crucial in achieving synergistic anticancer effects along with the other therapeutic molecules. In a recently published literature, investigators found that α-TOS enhances the anti-tumor activity of pterostilbene in human breast cancer cells in vivo and in vitro. Pterostilbene (dietary supplement) in association with α-TOS found to synergistically maximize the cytotoxicity to breast cancer cells, by disrupting signal transduction, transcription factors, and cell cycle proteins [30].

The present investigation was aimed to design the combined, synergistic and targeted therapy as a novel treatment strategy for TNBC by utilizing the HA (as CD44 receptor targeting ligand), α-TOS (to produce a synergistic anticancer effect) and Dox (as chemotherapeutic agent) delivered via MWCNTs as drug delivery platform. This strangely will be beneficial for the treatment of TNBC over the alone chemotherapy or surgery or a combination of both. The core objective behind the development of multifunctional MWCNTs was to achieve maximum therapeutic effects in MDA-MB-231 cells while reducing the associated side effect by chemotherapy alone. In a step by step synthesis, pristine MWCNTs were converted to aminated MWCNTs following successful carboxylation and acylation in different stages. Afterward, aminated MWCNTs were reacted with α-TOS-PEG-COOH and HA-PEG-COOH which were prepared by reacting α-TOS and HA with NH_2-PEG-COOH, using well-known NHS-EDC coupling chemistry in a separate reactions. Dox was loaded into finally obtained α-TOS-HA-MWCNTs conjugate to get α-TOS-HA-MWCNTs/Dox. The modified MWCNTs, as obtained from different steps, were characterized for their size, polydispersity index (PDI), surface charge, and surface morphology. Drug release was determined in acidic pH (5.0) in addition to normal physiologic pH (pH 7.4). The anti-cancer potential was assessed using the sulforhodamine B (SRB) assay and apoptotic assay. Cellular uptake of α-TOS-HA-MWCNTs was compared with non-HA functionalized formulations to determine the targeting efficiency of HA. Besides, hemocompatibility of different modified MWCNTs formulations were determined to be used as parenteral formulation.

2. Experimental section

2.1. General experimental materials and cell culture materials

Doxorubicin Hydrochloride (Dox) was obtained as gift from Sun Pharmaceuticals, Vadodara, India. Pristine multi-walled carbon nanotubes (Pristine MWCNTs; Purity > 98%, length 3-8 μm, and diameter 10–20 nm), α-Tocopheryl succinate (α-TOS) and Poly (Ethylene Glycol)- 2- Amino Ethyl Ether Acetic Acid (COOH-PEG-NH_2) (MW 2100 Da) were procured from Sigma Aldrich, India. Polytetrafluoroethylene (PTFE) filters (0.22 μm and 0.45 μm pore size) were purchased from Rankem, India. Hyaluronic acid (HA) and N-Hydroxy succinimide (NHS) were purchased from Alfa Aesar, India. Ethylene Diamine (EDA), 1-Ethyl-3-(3-dimethylaminopropyl) carbodiimide hydrochloride (EDC), Dimethyl Sulfoxide (DMSO), Dimethylformamide (DMF), Thionyl chloride ($SOCl_2$) and Dialysis Membranes (12–14 kDa and 1–2 kDa) were obtained from Himedia Pvt. Ltd. Mumbai, India. All other reagents and chemicals were of analytical grade and obtained from commercial sources. MDA-MB-231 cells received from National center for cell science (NCCS), Pune, India. Sodium bicarbonate (Product code TC230-100G), Dulbecco's Modified Eagle Medium (DMEM; Product code AT007F-5 L), antibiotic antimycotic solution 100× liquid, (Product code A002–20 ml; 10,000 U Penicillin, 10 mg Streptomycin and 25 μg Amphotericin B per ml in 0.9% normal saline), Trypsin-EDTA Solution 1× (Product code TCL007–500 ml) and Trypsin with 0.02% EDTA in Dulbecco's Phosphate Buffered Saline without phenol red (Product code TS1006) were procured from HiMedia Laboratories Pvt. Ltd., Mumbai, India. Fetal Bovine Serum (Heat inactivated, E.U. approved, Catalog number 10500064) was purchased from Gibco, Thermo Fisher Scientific, Bengaluru, India. Tris Buffer AR, molecular biology grade, 99.9%, (product code 71033) and Trichloroacetic acid extra-pure, 99% (product code 90544) were purchased from SRL Laboratories, Chennai, India. Sulphorhodamine B dye was purchased from MP Biomedicals, Singapore). Annexin V conjugated with Alexa Fluor 488 kit (Catalog #V13241) was obtained from Thermo Fisher Scientific, Bengaluru, India. Other materials such as ethanol, MilliQ water, NaOH, HCl, acetic acid were obtained from HiMedia Laboratories Pvt. Ltd., Mumbai, India.

2.2. Carboxylation of pristine MWCNTs

Initially, pristine MWCNTs (100 mg) were oxidized using oxidation method by dispersing in a 3 parts of H_2SO_4 and 1 part of HNO_3 (*v*/v) using ultrasonication (Sonapros PR-250MP, Oscar Ultrasonics Pvt. Ltd., Mumbai, India) for 5 min [31]. After that; the dispersion subjected to reflux at 80 °C employing a hotplate cum magnetic stirrer (Digital Round-Top Ceramic coated, Cole Parmer, Mumbai, India) at 900 rpm for 3 h. Then, the obtained dispersion of MWCNTs was diluted up to 6 times of its volume and washed using cooling centrifugation (−20 °C; C-24 Plus, Remi Elektrotechnik Ltd., Mumbai, India) at 10000 rpm 15 min. Washing was then carried out to remove traces of acid until pH reaches in between 5.0 **and** 6.0. Next, acetone (2 mL) was used to disperse oxidized MWCNTs and finally centrifuged at 10000 rpm. Then, the supernatant was discarded, and the final product was air-dried to get a fine powder of oxidized/carboxylated MWCNTs.

2.3. Acylation of carboxylated MWCNTs

Carboxylated MWCNTs (70 mg) was dissolved in 20 parts of thionyl chloride ($SOCl_2$) and 1 part of Dimethylformamide (DMF) at 70 °C for 24 h under stirring at 300 rpm [32]. After that, the acylated MWCNTs were washed with anhydrous tetrahydrofuran (THF) via centrifugation at 10000 rpm for 5 min for about six times till excess of $SOCl_2$ was removed. The obtained dark black residues were dried (Vacuum oven; Jyoti-Scientific Industries, Gwalior, India) at room temperature (RT) overnight for further use.

2.4. Amination of acylated MWCNTs

For amination of acylated MWCNTs, the dried acylated MWCNTs (50 mg) were added in a round bottom flask to react with two molar excess of EDA at 100 °C for three days until no hydrogen chloride gas was evolved [33]. The treated MWCNTs were subjected to washing with ethyl alcohol (2 mL) for several times until spare of EDA was

removed. The aminated MWCNTs were filtered using PTFE filters and dried in a vacuum oven at RT for 24 h to get solid powder for further use.

2.5. Conjugation of α-TOS to NH_2-PEG-COOH

The carboxyl groups of α-TOS (12.1 mg; 0.0225 mmol) were activated using EDC (4.31 mg, 0.0225 mmol) and NHS (4.89 mg, 0.0225 mmol) (pre-dissolved in 2 mL DMSO) for 180 min under magnetic stirring at 300 rpm [34]. After that, the activated α-TOS (1.5 **M** equivalents) was added gradually (in dropwise manner) to NH_2-PEG-COOH (29 mg; 0.015 mmol) dissolved in 5 mL of DMSO) under magnetic stirring (700 rpm). The stirring was kept continued for 24 h to complete the reaction. Then the mixture in reaction vessel was dialyzed against phosphate buffer saline (PBS) for three days and with water for another three days employing a dialysis membrane (MWCO 1–2 kDa) to eliminate the reactants in excess, followed by freeze-drying (FD8508; IIShinBioBase; South Korea) to obtain α-TOS-PEG.

2.6. Conjugation of HA to NH_2-PEG-COOH

The carboxyl groups of HA (8.1 mg; 0.0255 mmol) were activated using EDC (4.31 mg, 0.0225 mmol) and NHS (4.89 mg, 0.0225 mmol) (pre-dissolved in 2 mL DMSO) for 180 min under magnetic stirring at 300 rpm. Next, the activated HA was gradually added to NH_2-PEG-COOH (29 mg; 0.015 mmol) under magnetic stirring (700 rpm). The stirring was kept continued for 24 h for complete reaction. After that, the reaction mixture was purified by dialyzing against phosphate buffer saline (PBS) for 48 h and with water for another 24 h using a dialysis membrane (MWCO 1–2 kDa), followed by freeze-drying to obtain HA-PEG.

2.7. Conjugation of α-TOS-PEG and HA-PEG to aminated MWCNTs to obtained α-TOS-HA-MWCNTs

The carboxyl groups of α-TOS-PEG (9.3 mg) were activated by reacting with 2.5 **M** equivalents of EDC (15.1 mg, 0.1872 mmol) and NHS (16.2 mg, 0.1872 mmol) as coupling agents (in 3 mL DIW) for 2 h under magnetic stirring at 300 rpm. Similarly, carboxyl groups of HA-PEG (7.3 mg) were activated by reacting with 2.5 **M** equivalents of EDC (17.2 mg, 0.1879 mmol) and NHS (19.1 mg, 0.1879 mmol) as coupling agents (in 3 mL DIW) for 2 h under magnetic stirring at 300 rpm. Then, the carboxyl-activated α-TOS-PEG and HA-PEG was dropwise added to aminated MWCNTs (30.1 mg in 5 mL DIW) under vigorous magnetic stirring. The stirring process was continued for 24 h to complete the reaction. Then, the reaction mixture was purified by dialyzing against phosphate buffer saline (PBS) for 48 h and with water for another 24 h using a dialysis membrane (MWCO 12–14 kDa), followed by freeze-drying to obtain purified α-TOS-HA-MWCNTs.

2.8. Characterization of different MWCNTs conjugates

2.8.1. Fourier transform infrared (FTIR) spectroscopy

The FTIR spectroscopy for carboxylated MWCNTs, acylated MWCNTs, aminated MWCNTs, plain α-TOS, plain HA, plain Dox, α-TOS-MWCNTs, HA-MWCNTs, and α-TOS-HA-MWCNTs were carried out using KBr pellet method using FTIR spectrophotometer (Prestige-21; Shimadzu Corporation, Tokyo, Japan) at scanning range between 4000 **and** 650 cm^{-1}.

2.8.2. ^1H nuclear magnetic resonance (^1H NMR) spectroscopy

^1H NMR spectrum of carboxylated MWCNTs, acylated MWCNTs, aminated MWCNTs, plain α-TOS, plain HA, α-TOS-MWCNTs, HA-MWCNTs and α-TOS-HA-MWCNTs recorded using AV500 nuclear magnetic resonance spectrometer (Bruker Biospin, Rheinstetten,Germany). All samples were processed using D_6-DMSO before measurement.

2.8.3. X-ray diffraction (XRD) analysis

XRD analysis of carboxylated MWCNTs, acylated MWCNTs, aminated MWCNTs and α-TOS-HA- MWCNTs was carried out using XRD (MINIFLEX, Rigaku, Japan) employing HPAD detector. High-resolution XRD patterns were obtained by a scintillation counter (λ = 1.5406 Å) at a voltage of 30 kV and 10 mA, and diffraction values were measured at 2θ values between −3 to 145°.

2.9. Drug loading

For Dox loading, equilibrium dialysis method was adapted with slight modifications as reported earlier [35]. Briefly, Dox (1 mg/mL) was solubilized in acetone and aqueous triethylamine (TEA) solution in a 2:1 **M** ratio (Dox.TEA). Then the solution was stirred magnetically for 30 min. TEA was added to convert the salt form (hydrochloride) of Dox into its free form which was required to increase the Dox loading into different modified MWCNTs. Then, Dox (1 mg/mL) was loaded into α-TOS-HA-MWCNTs in phosphate buffer saline (pH 7.4) in the ratio of 2:1 by stirring for 48 h at RT in dark conditions. The finally obtained α-TOS-HA-MWCNTs/Dox subjected to centrifugation (5000 rpm) to remove unbound/free drug until the solution becomes colorless. A similar procedure was adopted during the Dox loading into aminated MWCNTs, α-TOS-MWCNTs and HA-MWCNTs. Dox loading was calculated by analyzing supernatant spectrophotometrically at 476 nm. Dox loaded formulations were then lyophilized and stored at 2–8 °C until further use. % loading efficiency was calculated using the following Eq. (1).

$$\%Loading\ efficiency = \frac{WLD - WFD}{WLD} \times 100 \quad (1)$$

where, WLD is the weight of loaded Dox, and WFD is the weight of free Dox.

2.10. Surface characterization

2.10.1. Size, polydispersity index, and surface charge determination

Different formulations viz. carboxylated MWCNTs, aminated MWCNTs, α-TOS-MWCNTs/Dox, HA-MWCNTs/Dox, and α-TOS-HA-MWCNTs/Dox was characterized upon the size, polydispersity index (PDI) and surface zeta potential. Malvern zeta sizer (Nano ZS90; Malvern Instruments, Ltd., Malvern, U.K.) was employed for the measurement of size and PDI using 170° backscattering based on the fundamentals of dynamic light scattering. Different formulations were appropriately diluted using DI water before analysis. Surface zeta potential was analyzed employing the same instrument based on the fundamentals of electric mobility. Separate cuvettes were used for an average size, PDI, and surface electric charge measurements.

2.10.2. Surface topography using transmission electron microscopy (TEM)

The surface of the Pristine MWCNTs, aminated MWCNTs, α-TOS-MWCNTs/Dox, HA-MWCNTs/Dox, and α-TOS-HA-MWCNTs/Dox was characterized for shape and structural visualization using TEM (TECNAI 200 Kv; Fei, Electron Optics, Oregon, USA).

2.11. In vitro drug release studies

In vitro release of Dox from α-TOS-HA-MWCNTs/Dox was carried out in phosphate buffer saline (pH 7.4) and acetate buffer (pH 5.0) as the recipient media to mimic the usual physiological milieu and lysosomal pH, respectively. Dox-loaded MWCNTs dispersion was prepared and filled in a dialysis bag with an MWCO of 12–14 kDa which was hermetically sealed from both the ends. The dialysis membrane filled dispersion was immediately placed in the receptor compartment, containing the recipient media. The sink conditions were maintained with

constant stirring and temperature kept at 37 ± 0.5! Digit expected.0.5 °C. Aliquots (1 mL) were withdrawn at pre-determined time (1, 2, 4, 6, 8, 12, 24, 48, 72, 96 and 120 h) and after the withdrawal of aliquots, the recipient media was replenished with the similar volume of buffer solution (1 ml). The concentration of released Dox was estimated using UV–Visible spectrophotometer at 476 nm plotting calibration curve and extrapolating the value on the curve.

2.12. Cytotoxicity assay using SRB dye

Cytotoxic potential of different modified MWCNTs formulations was evaluated on MDA-MB-231 cells employing the sulforhodamine B (SRB) assay. Cells were trypsinized and seeded in 96-well plates at a density of 5000 cells/well for 24 h. Then, the cells were incubated for 48 h with 0.01–100 μg/ml of each compound dissolved in Milli-Q water followed by fixing using 50 μl of cold 50% (*w/v*) TCA. Then, the cells were incubated for 60 **min** at 4 °C. After washing the plates using PBS, cells were treated with SRB (50 μL) at 0.04% (w/v) in 1% acetic acid and further incubated for 60 min at RT. After that, the residual dye was eliminated by several washing with 1% (*v*/v) acetic acid, following the air-drying of plates. Subsequently, the bound stain was eluted using 10 mM Tris base (pH 10.5) and the absorbance was taken at 490 nm. The concentrations that caused a 50% reduction in cell growth (GI_{50}) was estimated using a non-linear regression method from the concentration-response curve between concentration versus % GI_{50} via GraphPad Prism software (version 5.01 for Windows; GraphPad Software Inc., USA).

2.13. Cellular uptake analysis

MDA-MB-231 cells were seeded (2.5×10^5 cells per 12-well plate) and incubated for 24 h. After that, cells were treated with GI_{50} concentration of control, plain Dox, aminated MWCNTs/Dox, α-TOS-MWCNTs/Dox, HA-MWCNTs/Dox, α-TOS-HA-MWCNTs/Dox for 24 h. After 24 h media was aspirate out and washed using PBS two times. Next, cells were stained with 4′,6-diamidino-2-phenylindole (DAPI) at a concentration of 5 μg/mL for 30 min at RT. The morphological changes in the nucleus were finally visualized using confocal laser scanning microscope (CLSM: Leica TCS SP5 AOBS, Leica, Germany) at an excitation and emission wavelength of 365 nm/460 nm, respectively.

2.14. Apoptotic assay using Alexa Fluor® 488 kit

MDA-MB-231 cells were plated (density; 2.5×10^5 cells per 12-well plate) and incubated for 24 h. After 24 h, cells were again incubated with GI_{50} concentration of control, plain Dox, aminated MWCNTs, α-TOS-MWCNTs, HA-MWCNTs, α-TOS-HA-MWCNTs for 24 h. After that, cells were treated using annexin V conjugated with Alexa Fluor® 488 kit (Catalog #V13241, Thermo Fisher Scientific) to determine degree of apoptosis by addition of 100 μL of 1 × binding buffer + 5.0 μl Alexa Fluor® 488 Annexin V + 1.0 μl PI (100 μg/ml PI) to each well. Samples were mixed gradually and further subjected to incubation under dark for 15 min at RT. After the incubation period, 300 μL 1 × binding buffer added to each sample and immediately flow cytometric analysis (S3e™ Cell Sorter, Bio-Rad, United States) was carried out. 10,000 cells within the gated region were analyzed as a minimum number of cells.

2.15. Hemocompatibility assay

The hemocompatibility assay of plain Dox, aminated MWCNTs, α-TOS-MWCNTs, HA-MWCNTs, and α-TOS-HA-MWCNTs was carried out at their GI_{50} concentration following the previously reported protocols [36,37]. Briefly, mouse blood was transferred in heparinized storage vials and then centrifuged at 2000 rpm for 15 min to obtained RBCs separately from the blood. After washing, the collected RBCs used to prepare positive (100% hemolysis) and negative control (No hemolysis) using triton (10% *v*/v) and normal saline, respectively. Different formulations Dox, aminated MWCNTs, α-TOS-MWCNTs, HA-MWCNTs, and α-TOS-HA-MWCNTs/Dox were added separately to the 2% v/v RBC suspension following 2 h gentle shaking using an orbital shaker and then centrifuged at 2500 rpm for 10 min to collect the supernatant. Supernatants were then analyzed for absorbance using UV visible spectrophotometer at 540 nm. The % hemolysis was obtained following Eq. (2).

$$\%\text{Haemolysis} = \frac{\text{Absorbance of sample} - \text{Absorbance of blank}}{\text{Absorbance of positive control} - \text{Absorbance of blank}} \times 100 \quad (2)$$

2.16. Stability evaluation of α-TOS-HA-MWCNTs/Dox

The stability of different Dox loaded MWCNTs viz. aminated MWCNTs, α-TOS-MWCNTs, HA-MWCNTs and α-TOS-HA-MWCNTs were analyzed in the dispersed form (100 mg/mL) after lyophilization employing 2%*w/v* trehalose. Stability was assessed at 5 ± 1 °C and 30 ± 2 °C for 90 days and stability was measured based on changes in average particle size of different MWCNTs at predetermined intervals of 0, 7, 14, 30, 60 and 90 days. Besides, to know the suitable container type (Transparent or amber colored vials) for final packaging of α-TOS-HA-MWCNTs/Dox, it was stored in transparent and amber-colored tightly closed glass vials at 5 ± 1 °C and 30 ± 2 °C for 90 days in stability chambers dually following the guideline of International Conference on Harmonization (ICH) of Technical Requirements for Registration of Pharmaceuticals for finished pharmaceutical drug products. Observations were made as a function of change in organoleptic properties like precipitation, turbidity, color and viscosity changes.

2.17. Statistical analysis

Statistical analysis for experiments conducted was measured using a one-way analysis of variance (ANOVA) with a Tukey–Kramer multiple comparison Post-test and two-way ANOVA with Bonferroni post-test to match by GraphPad Prism 6.01TM software (GraphPad Software Inc., USA). A probability level of $p < .05$, $p < .01$ and $p < .001$ was assumed to be significant and highly significant and values greater than that considered as non-significant ($p > .05$).

3. Results and discussion

3.1. Carboxylation, acylation and amination of MWCNTs

Efficient, safe and targeted therapy is of paramount importance in treating TNBC and the current focus area for the development of the majority of nanomedicines for TNBC treatment [38]. In the last couple of years, among the carbon-based materials for delivery of small therapeutic molecules, MWCNTs have explored extensively owing to their excellent properties such as high drug loading and mechanical strength. MWCNTs are widely reported to be used in nanotechnology for theragnostic applications. The main restriction behind the use of CNT is their natural high hydrophobicity, which leads to accumulation and thereby produces toxicity. MWCNTs are reported to produce severe pulmonary toxicity associated with their inorganic residues, shape, size and diameter. Particularly, in cancer, high length of MWCNTs may restrict them to reach desired site (cancer cells) and therefore may result into toxicity. As a solution to lessen their toxicity, surface functionalization in terms of carboxylation, acylation, and amination has reported widely [39]. Surface modification may result into increase in their suspendability/solubility in aqueous media due to the availability of carboxylic, phenolic, and lactone functional groups on the sidewall surface. In the present investigation, carboxylic groups to the ends were attached via the oxidation method using two different acids (H_2SO_4 and

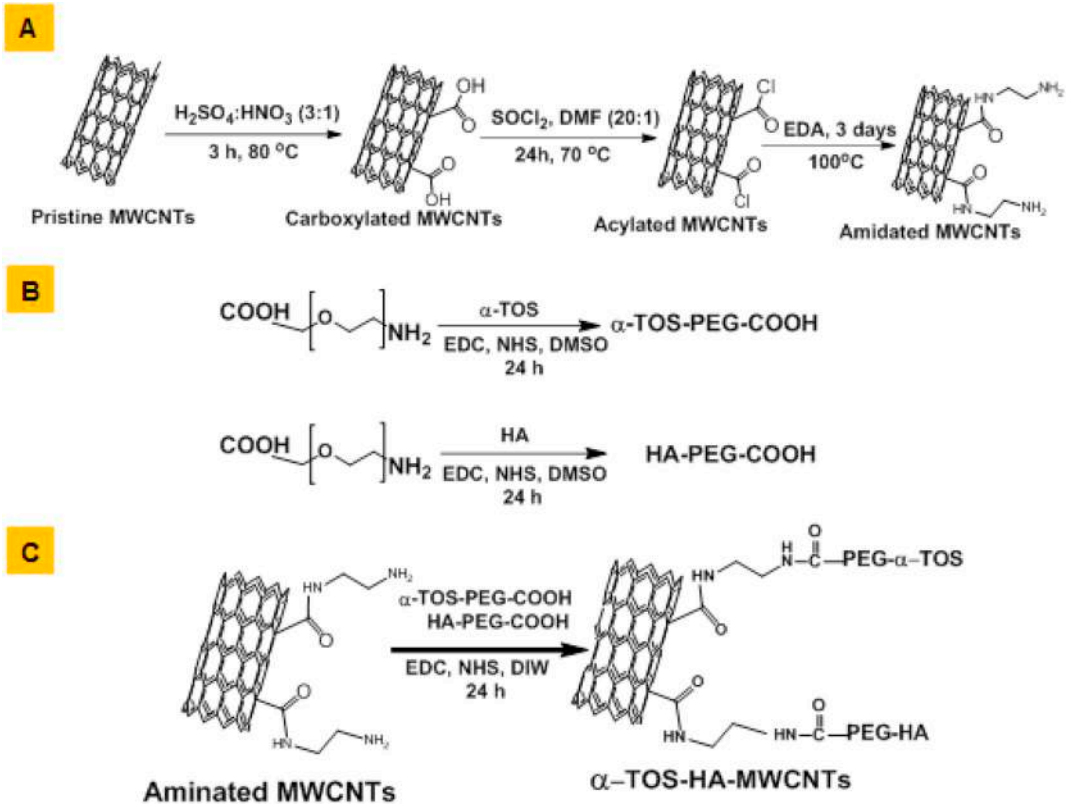

Fig. 1. Scheme showing different reaction steps involved in the formation of α-TOS-HA-MWCNTs. A. Aminated MWCNTs was obtained from pristine MWCNTs via mediating the formation of carboxylated MWCNTs and acylated MWCNTs. B. Next, α-TOS-PEG-COOH and HA-PEG-COOH were formed as an intermediate step. C. Finally, the α-TOS-HA-MWCNTs were formed upon initiating the reaction between aminated MWCNTs and α-TOS-PEG-COOH and HA-PEG-COOH.

HNO_3) as shown in Fig. S1A.

Next, carboxylated MWCNTs were reacted with the mixture of $SOCl_2$ and DMF to obtained acylated MWCNTs (Fig. 1A). After acylation, MWCNT was exposed to EDA for the attachment of amine groups and to obtained aminated MWCNTs (Fig. 1A). Considering that the cancerous cells have overexpression of CD44 receptors onto their surface, we aimed to utilize the HA as targeting ligand along with α-TOS to produce a synergistic effect. In a different reaction, COOH-PEG-NH_2 and α-TOS and HA was added separately (Fig. 1B). In a final step, α-TOS-PEG-COOH and HA-PEG-COOH were conjugated to aminated MWCNTs using well-established EDC/NHS coupling reagents chemistry to obtained α-TOS-HA-MWCNTs (Fig. 1C).

3.2. FTIR analysis

FTIR is a well-known and recognized technique for primary confirmation of conjugate formation, bond dissociation/formation and structural analysis based on functional group identification. FTIR spectrums for different formulations are shown in Fig. 2. Carboxylation of MWCNTs was confirmed by the peaks at 3437 cm^{-1} and 1699 relating to the O—H and C═O stretching. Acylation was confirmed by peaks at 2900 cm^{-1} (C—H stretching) and 780 cm^{-1} (C—Cl stretching), while amination was verified by observing the peaks at 3350 cm^{-1} and 1331 cm^{-1} for N—H and C—H stretching, respectively. Additionally, C═O cm^{-1} stretching of amide was recorded at 1661 cm^{-1} further confirmed the formation of an amide bond. Conjugation of PEG with α-TOS confirmed after getting peaks at 3441 cm^{-1}, 1756 cm^{-1}, and 1662 cm^{-1} corresponding to N—H stretching, C═O stretching of acid and C═O stretching of amide. Similarly, HA-PEG formation was confirmed by observing the peaks at 3348 cm^{-1}, 1757 cm^{1}, and 1670 cm^{-1} respectively for N—H stretching, C═O stretching of acid and C═O stretching of amide. Further conjugation of α-TOS-PEG and HA-PEG with aminated MWCNTs in two different reaction vessels was confirmed by identifying peaks located at 3448 cm^{-1}, 3288 cm^{-1}, 1136 cm^{-1} and 1066 cm^{-1}, respectively for N—H stretching and C—O stretching of ether. The successful conjugation of α-TOS-HA-MWCNTs was evident by the peaks at 3457 cm^{-1} (O—H stretching), 3412 cm^{-1} (N—H stretching) and 1616 cm^{-1} (C═O stretching; amide bond formation). Moreover, as shown in FTIR spectrum of α-TOS-HA-MWCNTs/Dox, the appearance of a peak at 1630 cm^{1} and the disappearance of the two peaks at 1580 cm^{-1} and 1610 cm^{-1} (N—H), which exist in Dox, verified the successful attachment of Dox.

3.3. ^{1}H NMR analysis

As a powerful tool for the determination of chemical structure, conjugate formation of complex structures, NMR was employed for the confirmation of different modified MWCNTs structures. Different NMR spectrum pertaining to MWCNTs modification was depicted as Fig. S1. The conversion of MWCNTs to carboxylated MWCNTs do not show any change in proton signal, as observed in other literatures as well [28]. Further, amination leads to formation of CH_2– proton signals around 1–3 ppm correspond to amine conjugation as seen in the spectrum of the aminated MWCNTs, confirms the formation of aminated MWCNTs. In the case of α-TOS, proton peaks were observed at 0.802–2.003 ppm and 2.489–2.798 ppm, related to 2 proton of methylene on the B position of benzene. For HA, peaks observed at 1.9–2.01 ppm and 3.30–4.79 ppm corresponds to acetamido moiety and methylene and hydroxyl groups of HA, respectively. Formation of α-TOS-PEG and HA-PEG was confirmed by observing the typical proton peaks at the region of 6.4–7.1 ppm. Further conjugation of α-TOS-PEG and HA-PEG to MWCNTs to obtained α-TOS-HA-MWCNTs was confirmed by the emergence of the typical proton peaks correspond to α-TOS and HA while shift at 3.25 ppm showed the presence of aromatic 1° amine groups.

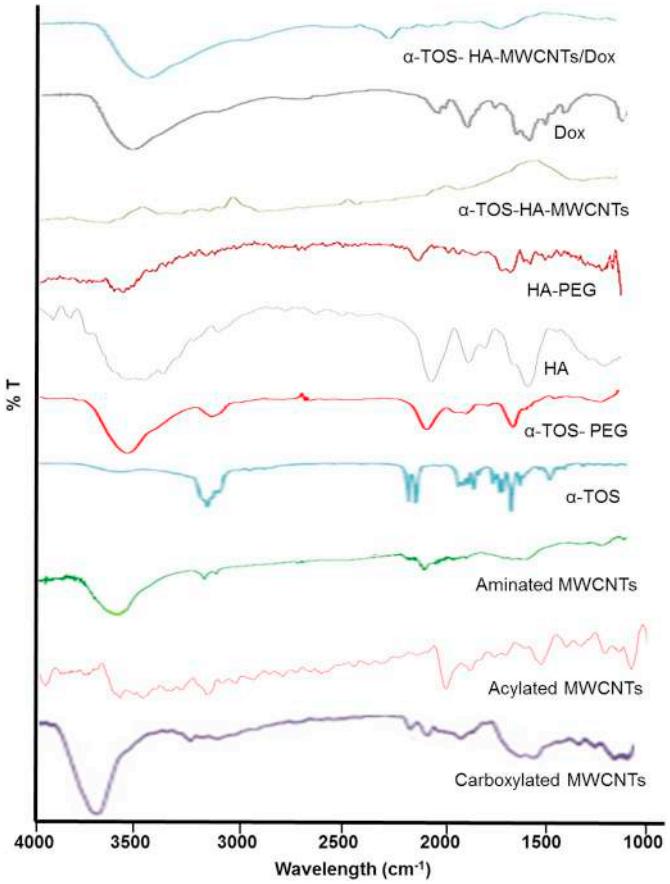

Fig. 2. FTIR analysis of carboxylated MWCNTs, acylated MWCNTs, aminated MWCNTs, α-TOS, α-TOS-PEG, HA, HA-PEG, Dox, α-TOS-HA-MWCNTs, α-TOS-HA-MWCNTs/Dox. FTIR was used as a spectroscopic tool for confirmation of conjugation/modification to MWCNTs.

3.4. XRD analysis

XRD was employed to know all possible diffraction directions of the lattice via the random orientation of the different modified MWCNTs formulations. The XRD graph of carboxylated MWCNTs revealed the peak at 25.3042 with an area of 734.39 (Fig. S2). Moreover, the XRD graph for aminated MWCNTs revealed the down-shifted peak at 22.1823, confirming the amination. Similarly, characteristic peaks for attachment of α-TOS and HA were observed and finally, the peaks at 14.7439, 18.8324, 21.9842, 20.9745, 29.9742 and 30.6432 confirmed the conjugation of α-TOS and HA to the aminated MWCNTs. Moreover, clear peak retention for both HA and α-TOS, indicating the successful conjugation with the aminated MWCNTs.

3.5. Surface characterization

3.5.1. Size, PDI and surface charge determination

Size and surface of the MWCNTs structures played a vital role in attaining the desired therapeutic effects. Different modified MWCNTs formulations were characterized on the basis of their size, PDI and surface charge using DLS by Zetasizer. As shown in Table 1, initial size of acids treated MWCNTs was found to be 149.0 ± 1.62 nm. Afterward, subsequent modification to obtained aminated MWCNTs/Dox, α-TOS-MWCNTs/Dox, and HA-MWCNTs/Dox leads to a gradual increase in size 158.0 ± 0.96 nm, 167.0 ± 0.17 nm and 171.2 ± 0.38 nm, respectively. These slight changes could be ascribed by change in ligand and Dox loading. However, almost 46.5% enhancement in size was observed between the carboxylated MWCNTs and finally obtained α-TOS-HA-MWCNTs/Dox (222.8 ± 1.13). The findings revealed that subsequent attachment of α-TOS and HA along with the Dox loading leads to a natural increase in size. PDI values were found between 0.3 **and** 0.1 for almost all the tested formulations (Table 1). PDI improves slightly from 0.309 ± 0.055 to 0.191 ± 0.085 from aminated MWCNTs/Dox to α-TOS-HA-MWCNTs/Dox ascribed the role of ligands in getting more homogeneous MWCNTs formulation. Also, surface charge shifts from negative side (−16.4 ± 1.4) to positive side (30.2 ± 1.2), when carboxylated MWCNTs converted to aminated MWCNTs/Dox, possibly due to attachment of -NH_2 on the outer ring of the nanotubes, which imparts the cationic charge. Moreover, surface charge continues to increase with the formation of α-TOS-MWCNTs/Dox (ζ; 35.8 ± 1.5) HA-MWCNTs/Dox (ζ; 32.7 ± 1.1) and α-TOS-HA-MWCNTs/Dox (ζ; 41.3 ± 1.2).

3.5.2. Determination of surface morphology using TEM

Surface morphology of modified MWCNTs was essential to determine considering their role in the material's properties. The surface morphology of pristine MWCNTs aminated MWCNTs, α-TOS-MWCNTs, HA-MWCNTs, α-TOS-HA-MWCNTs, α-TOS-HA-MWCNTs/Dox was observed using TEM. As compared to the TEM image of pristine MWCNTs, the surface seems to be reduced with aminated MWCNTs, probably due to the loss of metallic impurities resulted from successive carboxylation, acylation and amination (Fig. 3A and B). Surface coating in the case of α-TOS-MWCNTs and HA-MWCNTs was clearly visible as an effect of α-TOS and HA attachment (Fig. 3C and D). Moreover, the coating gets intense with α-TOS-HA-MWCNTs, displaying the successful attachment of both, α-TOS and HA on MWCNTs surface (Fig. 3E). Fig. 3F showed the Dox loading to α-TOS-HA-MWCNTs resulting from hydrogen bonding and hydrophobic interactions.

3.6. Drug loading

The Dox loading efficiency of α-TOS-HA-MWCNTs/Dox was calculated to be 76.23 ± 1.76% as determined following the equilibrium dialysis method. No significant difference ($p < .0001$) in the loading efficiency of α-TOS-MWCNTs (65.54 ± 2.13) and HA-MWCNTs (67.76 ± 2.98) was observed but found superior than aminated

Table 1
Size, PDI, surface charge and loading efficiency of carboxylated MWCNTs, aminated MWCNTs/Dox, α-TOS-MWCNTs/Dox, HA-MWCNT/Dox, and α-TOS-HA-MWCNTs/Dox.

Formulations	Size (nm) ± SD	PDI ± SD	Surface charge ± SD (ζ; mV)	Loading efficiency (%) ± SD
Carboxylated MWCNTs	149.0 ± 1.62	0.320 ± 0.031	−16.4 ± 1.4	–
Aminated MWCNTs/Dox	158.0 ± 0.96	0.309 ± 0.055	30.2 ± 1.2	56.25 ± 1.77
α-TOS-MWCNTs/Dox	167.0 ± 0.17	0.155 ± 0.062	35.8 ± 1.5	65.54 ± 2.13
HA-MWCNTs/Dox	171.2 ± 0.38	0.117 ± 0.041	32.7 ± 1.1	67.76 ± 2.98
α-TOS-HA-MWCNTs/Dox	222.8 ± 1.13	0.191 ± 0.085	41.3 ± 1.2	76.23 ± 1.76

Different modified MWCNTs formulations were characterized based on their size, PDI and zeta potential (ζ) using DLS by Zetasizer. The findings were important to know the size and surface properties such as surface charge and surface morphology. Results are represented as Mean ± SD (n = 3).

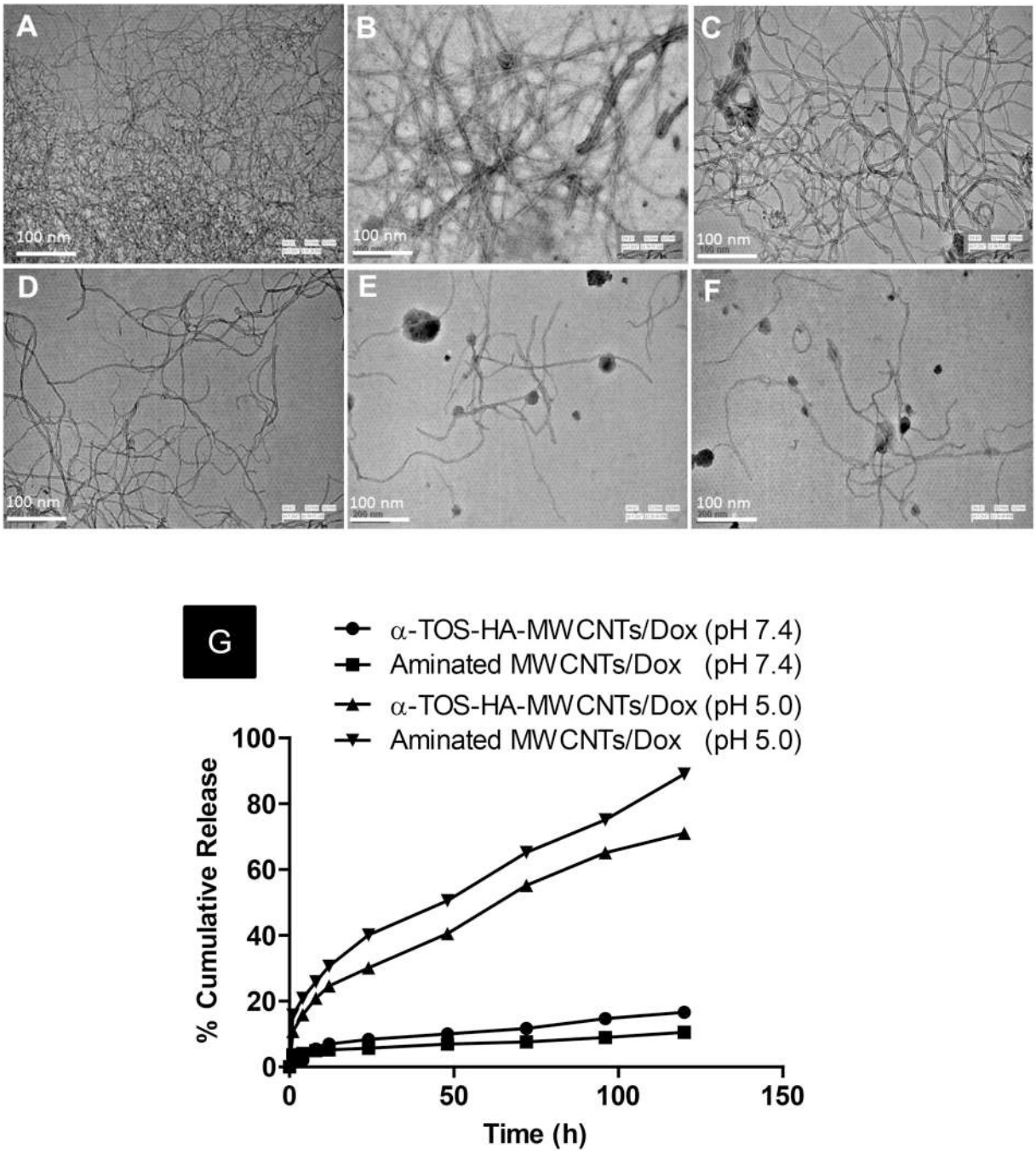

Fig. 3. TEM photomicrographs of (A) Pristine MWCNTs (B) Aminated MWCNTs (C) α-TOS-MWCNTs (D) HA-MWCNTs (E) α-TOS-HA-MWCNTs (F) α-TOS-HA-MWCNTs/Dox. TEM revealed the surface structural changes upon modifications such as conjugation with α-TOS, HA, α-TOS-HA and Dox. (G) Depiction of Dox release from aminated MWCNTs/Dox and α-TOS-HA-MWCNTs/Dox at two different pH viz PBS; pH 7.4 and acetate buffer; pH 5.0). Experiments were performed using a dialysis tube (MWCO 12–14 kDa), hermetically sealed at both ends. The release medium was kept on stirring for the entire duration of the experiment at 150 rpm at 37 ± 2 °C. After the predetermined intervals, 1 ml of media was taken and filled with the same amount of fresh medium to retain the sink conditions. Results are represented as Mean ± SD (n = 3).

MWCNTs. Similarly, in case of α-TOS-HA-MWCNTs/Dox dramatic improvement (almost 1.8×) in loading efficiency was observed as compared to aminated MWCNTs (56.25 ± 1.77; $p < .05$) (Table 1). The higher loading of Dox to α-TOS-HA-MWCNTs/Dox possibly involves π-π stacking, hydrogen bonding and hydrophobic interaction largely due to the aromatic ring structure of the Dox.

3.7. Drug release kinetics

The Dox release from α-TOS-HA-MWCNTs/Dox was determined in two different pH medium; PBS (pH 7.4) and sodium acetate buffer solution (pH 5.0) for the period of 120 h. Only 10.98 ± 1.01% and 16.87 ± 2.13% ($p < .05$) Dox was found released from α-TOS-HA-MWCNTs/Dox and aminated MWCNTs/Dox, under pH 7.4 (PBS) respectively, in 120 h (Fig. 3G). Whereas, Dox was found to release at a faster rate at pH 5.0, from α-TOS-HA-MWCNTs/Dox and almost 71.99 ± 2.34% drug was released in 120 h. In comparison, 89.98 ± 1.21% Dox was released during the same duration from aminated MWCNTs/Dox under similar conditions (Fig. 3G). Results indicated that the ligand HA, in combination with α-TOS, also

(A)

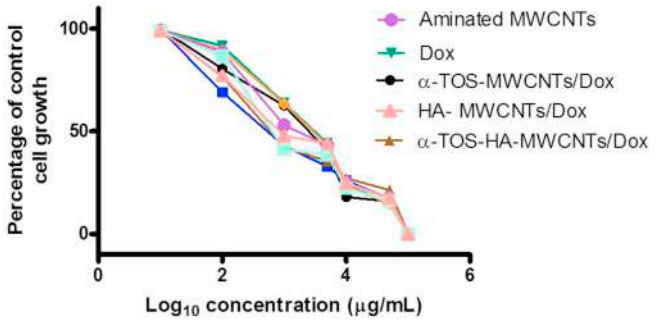

(B)

Formulations	Growth inhibition (GI_{50}) (μg/mL)
Aminated MWCNTs/Dox	1.957±0.042
Dox	2.621±0.153
α-TOS-MWCNTs/Dox	1.271±0.047
HA-MWCNTs/Dox	1.184±0.025
α-TOS-HA-MWCNTs/Dox	0.810±0.017

Fig. 4. SRB growth inhibition assay of MDA-MB-231 cells treated with aminated MWCNTs/Dox, plain Dox, α-TOS-MWCNTs/Dox, HA-MWCNTs/Dox and α-TOS-HA-MWCNTs/Dox at the Dox concentrations of 0–4 μM for 24 h. (A) Showing the graph of % Cell growth vs. Log10 concentration. (B) Growth inhibition GI_{50} values for different treatment groups. SRB assay, which is basically based on the interaction between SRB dye and the proteins via electrostatic complex formation. The measurement relies on the intensity of color and more the number of living cells in the suspension, more will be the amount of released dye and more will be the intensity. Results are represented as Mean ± SD (n = 6).

contributed for prolonging the release from the α-TOS-HA-MWCNTs/Dox. The findings suggested that release of Dox depend on the pH and as pH drops and reaches to ~5.0 (acidic conditions), release gets faster. As a fact, Dox is having pH-dependent hydrophilicity and breakdown of its daunosamine groups because of protonation at acidic condition was one of the reasons for its faster rate of release at pH 5.0. Another reason includes the interaction and cleavage of bonding as the π-π stacking interaction is stronger at basic conditions and weak at acidic pH, triggered the detachment of Dox from MWCNTs. This is particularly important and desirable as the pH of tumor microenvironment is acidic. The release rate displayed a non-linear pattern characterized by initial prompt release subsequently altered to sustained release pattern after certain time. Moreover, Dox release from aminated MWCNTs showed a faster rate in both the tested pH as compared to α-TOS-HA-MWCNTs/Dox. Besides, hydrophobic nature of MWCNTs also adds in sustaining the release of Dox from its architect. Our findings clearly indicated that pH-dependent release of Dox is advantageous in targeted chemotherapy to **tumor** cells. Results of the Dox release found in good correlation with the previously reported data by Singh et al. [35], in which authors showed the sustained release pattern of Docetaxel from MWCNTs for 72 h without noticing any burst release.

3.8. Cytotoxicity assay

The anti-**tumor** potential of different formulations viz**.** plain Dox, aminated MWCNTs/Dox α-TOS-MWCNTs/Dox, HA-MWCNTs/Dox and α-TOS-HA-MWCNTs/Dox were evaluated by SRB assay using MDA-MB-231 cell lines at a cell density of 5000 cells per well. Unlike MTT assay which depends on metabolic activity, SRB assay based on the stoichiometric binding of SRB dye to basic amino acids under slightly acidic conditions. The measurement relies on the intensity of color and more the number of living cells in the suspension, more will be the amount of released dye and more will be the intensity. GI_{50} values of all formulations were calculated and represented in Fig. 4A and B. As compared to other tested formulations, α-TOS-HA-MWCNTs/Dox displayed lowest GI_{50} values with high cytotoxicity. The findings revealed that plain Dox (GI_{50}; 2.621 ± 0.153; $p < .001$) or aminated MWCNTs/Dox (GI_{50}; 1.957 ± 0.042; $p < .001$) was not effective however functionalization with α-TOS or HA or both can provide effective treatment. In particular, attachment of both the ligands (α-TOS and HA) was more effective (GI_{50}; 0.810 ± 0.017; $p < .001$), as compared to α-TOS-MWCNTs/Dox (GI_{50}; 1.271 ± 0.047) and HA-MWCNTs/Dox (GI_{50}; 1.184 ± 0.025). This ascribed the effect of attachment of dual ligands (α-TOS and HA) on MWCNTs that provoke the cellular uptake of the α-TOS-HA-MWCNTs/Dox and thereby the maximum amount of Dox was made available to interact with the DNA base pairs. Enhanced localization of Dox via increased receptor medicated cell uptake leads to a reduction in the GI_{50} values and therefore decreased the cell viability in the groups treated with α-TOS-HA-MWCNTs/Dox. Alternatively, the effect of sonication and chemical functionalization of MWCNTs, which reduces the agglomeration/bundling, also contributed to enhanced therapeutic efficacy and cannot completely rule out. Researchers also reported the similar findings of cytotoxicity against breast cancer-specific MCF-7 cells using SRB assay, in which Paclitaxel was loaded in MWCNTs [40].

3.9. Cellular internalization experiment

Cellular uptake of ligand decorated MWCNTs; HA-MWCNTs and α-TOS-HA-MWCNTs were compared with aminated MWCNTs/Dox and plain Dox. Outcomes revealed that Dox and alone rarely enters into cells and therefore, unable to promote cellular uptake (Fig. 5). As compared to Dox, aminated MWCNTs/Dox succeed to internalize but with a weaker intensity. Internalization was improved with α-TOS-MWCNTs ($p < .001$) and found even better with HA-MWCNTs, revealing the role of HA for targeting. HA is well-known, targeting ligand act via binding with overexpressed CD44 receptors on MDA-MB-231 cells. In particular, more profound uptake was observed using α-TOS-HA-MWCNTs/Dox. The increased uptake might be due to the synergistic effect of α-TOS and HA, justifying the treatment effectiveness as determined using SRB assay with α-TOS-HA-MWCNTs/Dox. Prajapati et al. also reported the enhanced targeting and cellular internalization of gemcitabine delivered via MWCNTs in vitro (in HT-29 colon cancer cell line) and in vivo (in Sprague Dawley rats), employing HA as targeting ligand [19].

3.10. Apoptosis analysis

In cells treated with compound with GI_{50} concentration of different modified MWCNTs formulations for 24 h, the As shown in Fig. 6, a less total apoptotic ratio (TAR; early + late apoptosis) was observed (06.13 ± 1.4%; $p < .001$ and 15.34 ± 3.23%; $p < .001$) with plain Dox and aminated MWCNTs/Dox. Moreover, as compared to α-TOS-MWCNTs/Dox (21.61 ± 4.32), HA-MWCNTs/Dox displayed high TAR % (34.90 ± 5.93), might be due to enhanced cellular internalization that resulted into Dox cytotoxicity to MDA-MB-231 cells. Notably, α-TOS-HA-MWCNTs/Dox showed highest TAR % (52.69 ± 4.86%; $p < 001$) indicating that the nuclear fragmentation and condensation were higher when aminated MWCNTs given along with α-TOS and HA modification and containing Dox, as compared to other formulations. Our findings exhibited synergistic chemotherapeutic effects and treatment is more effective with α-TOS and HA containing MWCNTs. On a comparable basis, Wang et al., showed an enhanced rate of apoptosis (48.7%; $p < 0.001$) in MCF-7/Adr cell when treated using HA conjugated nanoparticles in comparison to non-conjugated nanoparticles [41].

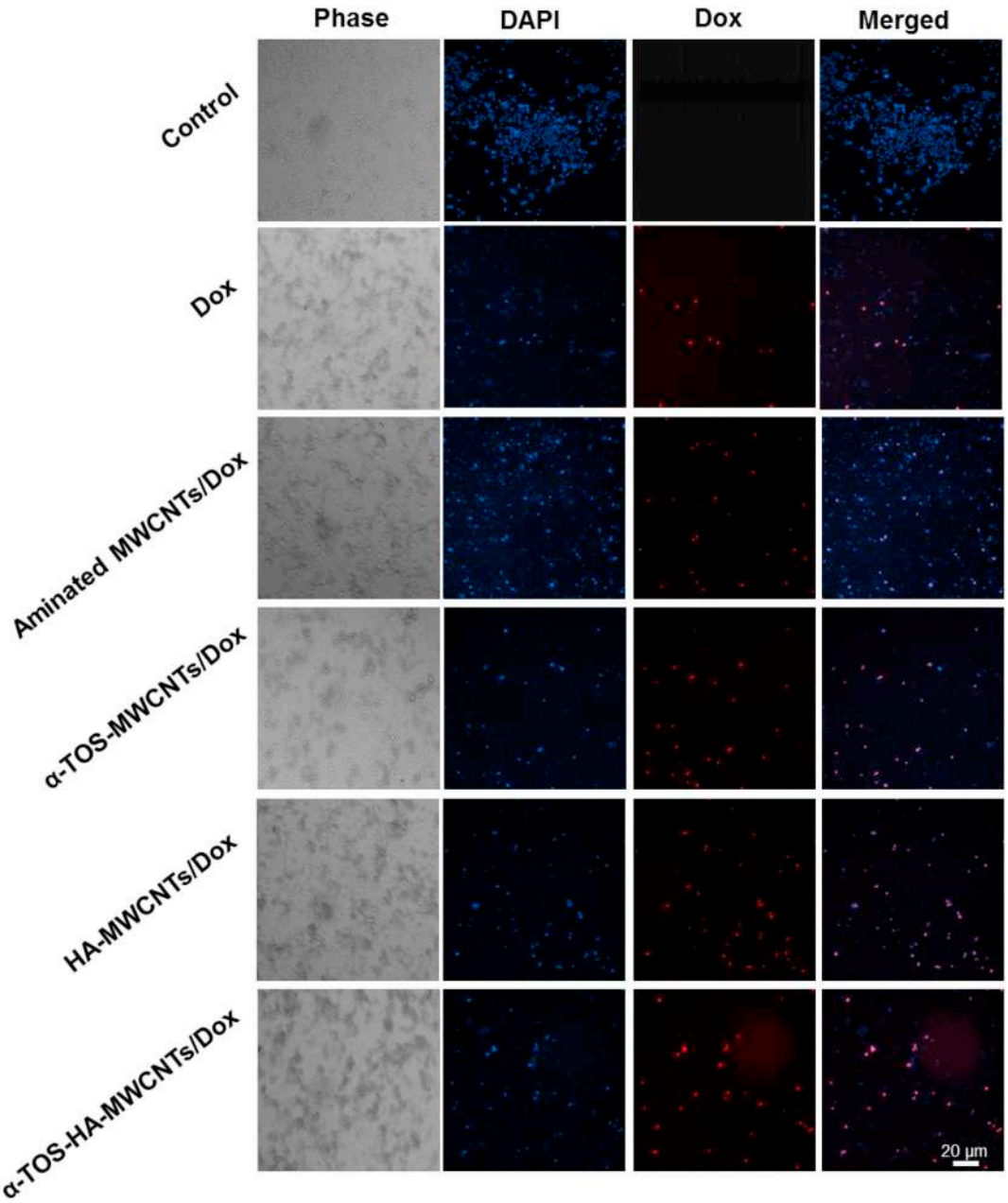

Fig. 5. Cellular internalization of aminated MWCNTs/Dox, plain Dox, α-TOS-MWCNTs/Dox, HA-MWCNTs/Dox and α-TOS-HA-MWCNTs/Dox observed in MDA-MB-231 cells. Cellular internalization was studied using CLSM to evaluate the alteration in cell uptake pattern before and after conjugation with HA, α-TOS. Scale bar: 20 μm.

3.11. Determination of blood compatibility

Hemocompatibility study was aimed to analyze the safety of different MWCNTs based formulations. Outcomes of hemocompatibility displayed safe nature of different MWCNTs, and all the formulations were found fewer than 2% hemolysis. Plain Dox (25 μg/mL) exhibited 2.01 ± 0.23% hemolysis, while aminated MWCNTs, α-TOS-MWCNTs, HA-MWCNTs and α-TOS-HA-MWCNTs/Dox 0.30 ± 0.34%, 1.21 ± 0.11%, 1.11 ± 0.24%, and 1.9 ± 0.35% respectively. The obtained values were indicative of safe nature of the formulations and unlikely to produce hemolysis ($p > .05$). The data also presented in Fig. 6B. Findings suggest the non-reactive nature of formulations upon interaction with blood components. This finding was in good agreement with that observed by Kumar et al., wherein *N*-desmethyl tamoxifen and quercetin-encrusted MWCNTs were reported to be safe upon interaction with blood components [42].

3.12. Stability analysis of α-TOS-HA-MWCNTs

During the stability analysis at 30 ± 1 °C, all the developed MWCNTs were found with significant increase ($P < .0001$) in size during the period of 90 days and aminated MWCNTs was found the most unstable formulation with 4.32 fold increment in size (from 158.0 ± 0.96 nm to 683.2 ± 7.89 nm). Similarly, as seen in Fig. 7A 3.55 fold, 3.24 fold and 2.20 fold increases in size was found respectively for α-TOS-MWCNTs, HA-MWCNTs and α-TOS-HA-MWCNTs during 90 days from their initial size. The finding showed that storage of different MWCNTs formulation is not recommended at 30 ± 1 °C. Stability analysis at 5 ± 1 °C, revealed that formulations were quite stable as compared to 30 ± 1 °C. Only 1.46 fold (from 158.0 ± 0.96 to 232.2 ± 8.15 nm), 1.34 fold (from 167.0 ± 0.17 to 222.7 ± 4.23 nm), and 1.33 fold (from 171.2 ± 0.38 to 232.1 ± 5.43) enhancement in average size was observed with

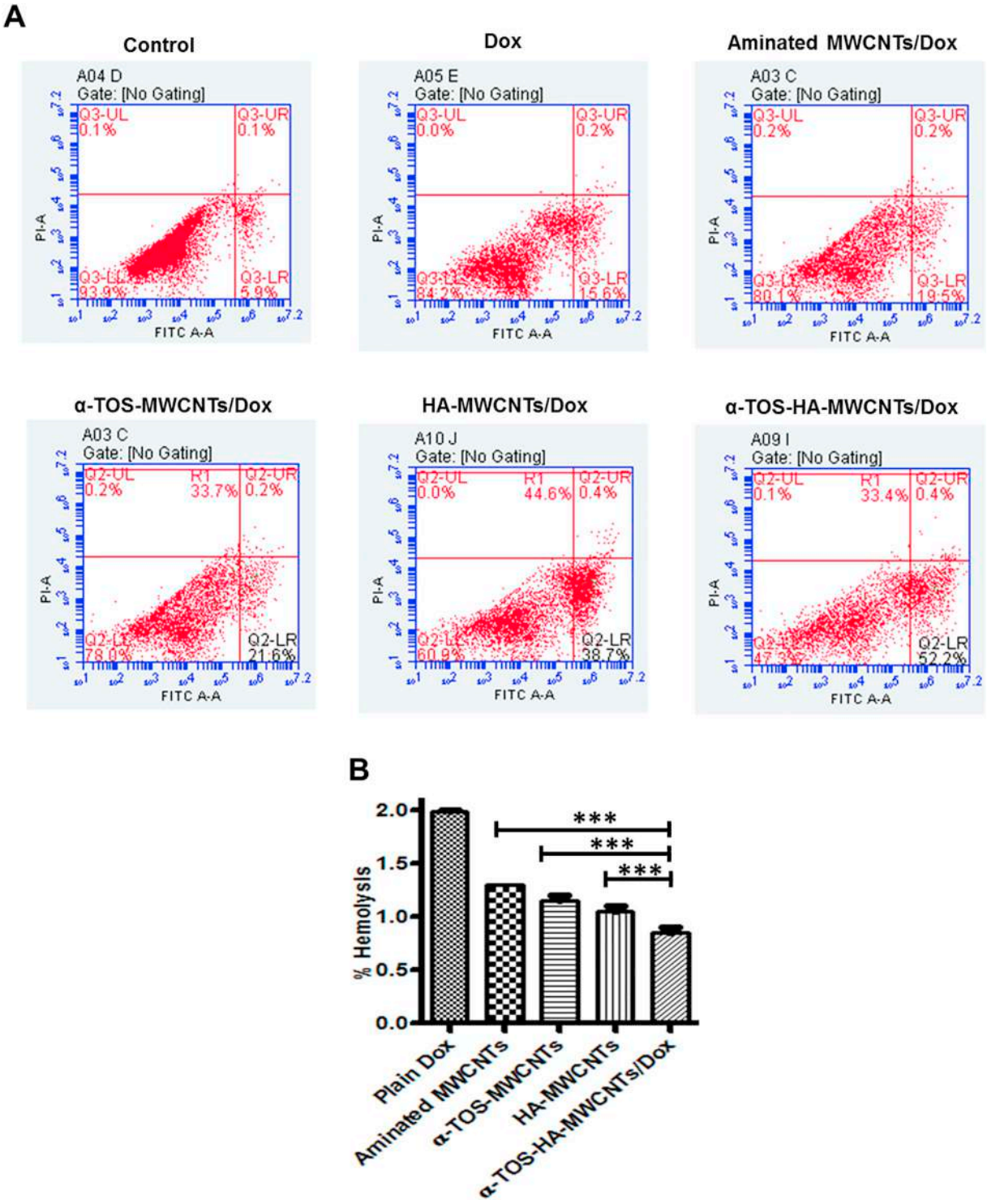

Fig. 6. (A) Apoptotic rate of MDA-MB-231 cells upon receiving treatment from different modified MWCNTs. For apoptosis analysis, Alexa Fluor®488 kit was used to stain the cells. Results are represented as mean ± S.D. (n = 6). (B) Hemocompatibility analysis of Plain Dox, aminated MWCNTs, α-TOS-MWCNTs, HA-MWCNTs, and α-TOS-HA-MWCNTs/Dox was carried out by withdrawing whole mouse blood collected in heparinized storage vials. Hemocompatibility study was aimed to analyze the safety of different MWCNTs modified formulations. Results are represented as Mean ± SD (n = 3).

aminated MWCNTs, α-TOS-MWCNTs and HA-MWCNTs, respectively (Fig. 7B). The data suggested that formulations were more stable at refrigerator temperature as compared 30 ± 1 °C. Increasing the temperature leads to nanotube aggregation, this eventually resulted in an increased particle size. Also, at higher temperature the bonding of the Dox with the nanotubes becomes unstable due to rise in thermal energy of the molecules. Findings suggest that at lower temperature (~ 5 °C), developed MWCNTs stable in dispersed form for 90 days being predominant with α-TOS-HA-MWCNTs/Dox with just 1.17 fold increase (222.8 ± 1.13 to 260.9 ± 7.12). The findings also suggest that modifying the surface of MWCNTs may result into enhancement in stability due to conjugate stabilization at refrigerator temperature. Our data on engineered MWCNTs are in accordance with the previously reported ones [43]. Moreover, data on suitable storage container

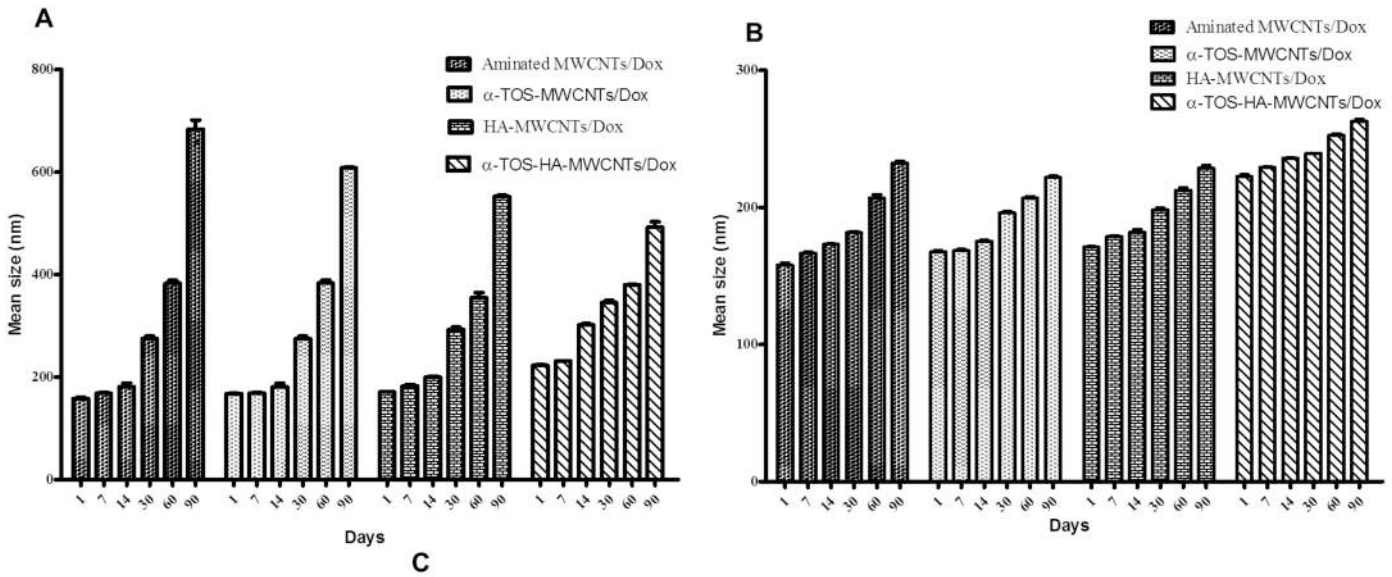

C

Type of vial	Transparent glass vial		Amber colored glass vial	
Temperature	5±1 °C	30±1 °C	5± 1°C	30± 1°C
Turbidity	++	+++	-	++
Precipitation	+	++	-	+
Color change	+	+	-	+

Fig. 7. Stability analysis of different modified MWCNTs at (A) 5 ± 1 °C and (B) 30 ± 1 °C in dispersed form in water. Stability study was conducted intermittently for 90 days. Measurements were based on the changes in particle size. (C) Results of storage stability test to determine the suitability of container type (Transparent and amber glass vials). Results are represented as Mean ± SD (n = 3). + Low + + Moderate + + + High.

revealed that storage in transparent glass vials at both the temperature conditions (5 ± 1 °C and 30 ± 1 °C) leads to turbidity, which might be due to nanotube agglomeration which could be attributed as light effect (Fig. 7C). Furthermore, storage in amber glass vial (light resistant vials) found promising as no sign of turbidity was seen at 5 ± 1 °C. However, slight turbidity was noted at 30 ± 1 °C, which might be due to temperature effect. Results interpreted that storage condition label for the α-TOS-HA-MWCNTs/Dox must include "store in a cool place away from light".

4. Conclusion

In this investigation, the CD44 receptor-targeted α-TOS and HA tailored and Dox loaded MWCNTs (α-TOS-HA-MWCNTs/Dox) with synergistic anticancer formulation was successfully prepared and characterized to serve against TNBC. Dox was utilized as a model anticancer therapeutic molecule for effective treatment. The strategy was to combine the anticancer potential of Dox, targeting potential of HA and synergistic effect of α-TOS to treat an aggressive form of breast cancer, TNBC. The in vitro anticancer potential determined synergistically by using Dox and α-TOS (α-TOS-HA-MWCNTs/Dox), resulted in higher therapeutic efficacy as compared to α-TOS-MWCNTs/Dox and HA-MWCNTs/Dox alone. Besides, anticancer potential of different modified MWCNTs was determined using apoptotic assay results of which were found in good agreement with those observed using SRB assay. An apoptotic assay using Alexa Fluor® 488 kit revealed the ablation/killing of > 85% MDA-MB 231 cells upon treatment with α-TOS-HA-MWCNTs/Dox. Blood compatibility assay of different modified MWCNTs revealed the safe nature of all the formulations as no notable hamolysis was seen. Moreover, stability investigation was conducted for assessing the correct storage temperature and correct type of glass vial. Storage in amber **colored** glass vial at refrigerator temperature was found appropriate to keep the developed MWCNTs for 90 days. The synergistic approach presented could also be applied for the intervention of other related ailments overexpressing CD44 receptors.

Declaration of Competing Interest

The authors declare that they have no known competing financial interests or personal relationships that could have appeared to influence the work reported in this paper.

Acknowledgements

Authors are deeply grateful to the Department of Science and Technology (DST), for providing research fund under women scientist program (SR/WOS-A/LS-314/2016) to Ms. Nidhi Jain Singhai. Authors would also thankful to the Rajiv Gandhi Technological University for providing necessary infrastructure and facility to carry out the experiments.

Appendix A. Supplementary data

Supplementary data to this article can be found online at https://doi.org/10.1016/j.colcom.2020.100235.

References

[1] G. Bianchini, J.M. Balko, I.A. Mayer, M.E. Sanders, L. Gianni, Triple-negative breast cancer: challenges and opportunities of a heterogeneous disease, Nat. Rev. Clin. Oncol. 13 (2016) 674.
[2] G. Prado-Vázquez, A. Gámez-Pozo, L. Trilla-Fuertes, J.M. Arevalillo, A. Zapater-Moros, M. Ferrer-Gómez, M. Díaz-Almirón, R. López-Vacas, H. Navarro, P. Maín, A novel approach to triple-negative breast cancer molecular classification reveals a luminal immune-positive subgroup with good prognoses, Sci. Rep. 9 (2019) 1538.
[3] H. Gonçalves Jr., M.R. Guerra, J.R. Duarte Cintra, V.A. Fayer, I.V. Brum, M.T. Bustamante Teixeira, Survival study of triple-negative and non–triple-negative breast cancer in a Brazilian cohort, Clin. Med. Insights Oncol. 12 (2018) 1179554918790563.

[4] Z. Sporikova, V. Koudelakova, R. Trojanec, M. Hajduch, Genetic markers in triple-negative breast cancer, Clin. Breast Cancer 18 (5) (2018) 841–850.
[5] S. Al-Mahmood, J. Sapiezynski, O.B. Garbuzenko, T. Minko, Metastatic and triple-negative breast cancer: challenges and treatment options, Drug Deliv. Transl. Res. 8 (2018) 1483–1507.
[6] V. Kulchitsky, A. Zamaro, V. Potkin, T. Gurinovich, S. Koulchitsky, Prospects of chemotherapy side effects minimization, Canc. Oncol. Open Access J. 1 (2018) 15–16.
[7] K. Ahmed, A. Koval, J. Xu, A. Bodmer, V.L. Katanaev, Towards the first targeted therapy for triple-negative breast cancer: **r**epositioning of clofazimine as a chemotherapy-compatible selective Wnt pathway inhibitor, Cancer Lett. 449 (2019) 45–55.
[8] A. Marra, G. Viale, G. Curigliano, Recent advances in triple negative breast cancer: the immunotherapy era, BMC Med. 17 (2019) 90.
[9] A.C. Garrido-Castro, N.U. Lin, K. Polyak, Insights into molecular classifications of triple-negative breast cancer: improving patient selection for treatment, Cancer Discov. 9 (2019) 176–198.
[10] N. Soni, N. Soni, H. Pandey, R. Maheshwari, P. Kesharwani, R.K. Tekade, Augmented delivery of gemcitabine in lung cancer cells exploring mannose anchored solid lipid nanoparticles, J. Colloid Interface Sci. 481 (2016) 107–116.
[11] R.K. Tekade, R. Maheshwari, N. Soni, M. Tekade, M.B. Chougule, Chapter 1 - **n**anotechnology for the **d**evelopment of Nanomedicine A2 - Mishra, Vijay, in: P. Kesharwani, M.C.I.M. Amin, A. Iyer (Eds.), Nanotechnology-Based Approaches for Targeting and Delivery of Drugs and Genes, Academic Press, 2017, pp. 3–61.
[12] R.G. Maheshwari, R.K. Tekade, P.A. Sharma, G. Darwhekar, A. Tyagi, R.P. Patel, D.K. Jain, Ethosomes and ultradeformable liposomes for transdermal delivery of clotrimazole: **a** comparative assessment, Saudi Pharm. J. 20 (2012) 161–170.
[13] R. Maheshwari, M. Tekade, P.A. Sharma, R.K. Tekade, Nanocarriers **a**ssisted siRNA **g**ene **t**herapy for the **m**anagement of **c**ardiovascular **d**isorders, Curr. Pharm. Des. 21 (2015) 4427–4440.
[14] P.A. Sharma, R. Maheshwari, M. Tekade, R.K. Tekade, Nanomaterial **b**ased **a**pproaches for the **d**iagnosis and **t**herapy of **c**ardiovascular **d**iseases, Curr. Pharm. Des. 21 (2015) 4465–4478.
[15] R.K. Tekade, R. Maheshwari, N. Soni, M. Tekade, Chapter 12 - **c**arbon **n**anotubes in **t**argeting and **d**elivery of **d**rugs A2 - Mishra, Vijay, in: P. Kesharwani, M.C.I.M. Amin, A. Iyer (Eds.), Nanotechnology-Based Approaches for Targeting and Delivery of Drugs and Genes, Academic Press, 2017, pp. 389–426.
[16] K. Kuche, R. Maheshwari, V. Tambe, K.K. Mak, H. Jogi, N. Raval, M.R. Pichika, R. Kumar Tekade, Carbon nanotubes (CNTs) based advanced dermal therapeutics: current trends and future potential, Nanoscale 10 (2018) 8911–8937.
[17] S. Mahajan, A. Patharkar, K. Kuche, R. Maheshwari, P.K. Deb, K. Kalia, R.K. Tekade, Functionalized carbon nanotubes as emerging delivery system for the treatment of cancer, Int. J. Pharm. 548 (1) (2018) 540–558.
[18] E. Arkan, R. Saber, Z. Karimi, M. Shamsipur, A novel antibody–antigen based impedimetric immunosensor for low level detection of HER2 in serum samples of breast cancer patients via modification of a gold nanoparticles decorated multiwall carbon nanotube-ionic liquid electrode, Anal. Chim. Acta 874 (2015) 66–74.
[19] S.K. Prajapati, A. Jain, C. Shrivastava, A.K. Jain, Hyaluronic acid conjugated multi-walled carbon nanotubes for colon cancer targeting, Int. J. Biol. Macromol. 123 (2019) 691–703.
[20] M. Liu, Y. Xu, C. Huang, T. Jia, X. Zhang, D.-P. Yang, N. Jia, Hyaluronic acid-grafted three-dimensional MWCNT array as biosensing interface for chronocoulometric detection and fluorometric imaging of CD44-overexpressing cancer cells, Microchim. Acta 185 (2018) 338.
[21] K. Kuche, P.K. Pandey, A. Patharkar, R. Maheshwari, R.K. Tekade, Hyaluronic **a**cid as an **e**merging **t**echnology **p**latform for **s**ilencing RNA **d**elivery, Biomaterials and Bionanotechnology, Elsevier, 2019, pp. 415–458.
[22] H.-Y. Seok, N.S. Rejinold, K.M. Lekshmi, K. Cherukula, I.-K. Park, Y.-C. Kim, CD44 targeting biocompatible and biodegradable hyaluronic acid cross-linked zein nanogels for curcumin delivery to cancer cells: **i**n vitro and in vivo evaluation, J. Control. Release 280 (2018) 20–30.
[23] L.Y. Bourguignon, Hyaluronan-mediated CD44 signaling activates cancer stem cells in head and neck cancer, Molecular Determinants of Head and Neck Cancer, Springer, 2018, pp. 525–544.
[24] O. Franklin, O. Billing, D. Öhlund, A. Berglund, C. Herdenberg, W. Wang, U. Hellman, M. Sund, Novel prognostic markers within the CD44-stromal ligand network in pancreatic cancer, J. Pathol.: Clin. Res. 5 (2019) 130–141.
[25] K. Härkönen, S. Pyysalo, S. Hakkola, K. Ketola, C. Oliveira, S. Oikari, K. Rilla, CD44 is a novel homing receptor for extracellular vesicles, J. Extracell. Vesicles 7 (2018) 103–104.
[26] G. Huang, H. Huang, Hyaluronic acid-based biopharmaceutical delivery and tumor-targeted drug delivery system, J. Control. Release 278 (2018) 122–126.
[27] H.J. Yao, L. Sun, Y. Liu, S. Jiang, Y. Pu, J. Li, Y. Zhang, Monodistearoylphosphatidylethanolamine-hyaluronic acid functionalization of single-walled carbon nanotubes for targeting intracellular drug delivery to overcome multidrug resistance of cancer cells, Carbon 96 (2016) 362–376.
[28] X. Cao, L. Tao, S. Wen, W. Hou, X. Shi, Hyaluronic acid-modified multiwalled carbon nanotubes for targeted delivery of doxorubicin into cancer cells, Carbohydr. Res. 405 (2015) 70–77.
[29] O.A. Ahmed, K.M. El-Say, B.M. Aljaeid, S.M. Badr-Eldin, T.A. Ahmed, Optimized vinpocetine-loaded vitamin e D-α-tocopherol polyethylene glycol 1000 succinate-alpha lipoic acid micelles as a potential transdermal drug delivery system: in vitro and ex vivo studies, Int. J. Nanomedicine 14 (2019) 33.
[30] K.-W. Tam, C.-T. Ho, S.-H. Tu, W.-J. Lee, C.-S. Huang, C.-S. Chen, C.-H. Wu, C.-H. Lee, Y.-S. Ho, α-Tocopherol succinate enhances pterostilbene anti-tumor activity in human breast cancer cells in vivo and in vitro, Oncotarget 9 (2018) 4593.
[31] D. Matyszewska, E. Napora, K. Żelechowska, J.F. Biernat, R. Bilewicz, Synthesis, characterization, and interactions of single-walled carbon nanotubes modified with doxorubicin with Langmuir–Blodgett biomimetic membranes, J. Nanopart. Res. 20 (2018) 143.
[32] H. Sadegh, G.A.M. Ali, S. Agarwal, V.K. Gupta, Surface **m**odification of MWCNTs with **c**arboxylic-to-**a**mine and **t**heir **s**uperb **a**dsorption **p**erformance, Int. J. Environ. Res. 13 (2019) 523–531.
[33] H.-j. Yao, Y.-g. Zhang, L. Sun, Y. Liu, The effect of hyaluronic acid functionalized carbon nanotubes loaded with salinomycin on gastric cancer stem cells, Biomaterials 35 (2014) 9208–9223.
[34] J. Zhu, L. Zheng, S. Wen, Y. Tang, M. Shen, G. Zhang, X. Shi, Targeted cancer theranostics using alpha-tocopheryl succinate-conjugated multifunctional dendrimer-entrapped gold nanoparticles, Biomaterials 35 (2014) 7635–7646.
[35] R.P. Singh, G. Sharma, S. Singh, M. Kumar, B.L. Pandey, B. Koch, M.S. Muthu, Vitamin E TPGS conjugated carbon nanotubes improved efficacy of docetaxel with safety for lung cancer treatment, Colloids Surf. B: Biointerfaces 141 (2016) 429–442.
[36] P.K. Pandey, R. Maheshwari, N. Raval, P. Gondaliya, K. Kalia, R.K. Tekade, Nanogold-core multifunctional dendrimer for pulsatile chemo-, photothermal-and photodynamic-therapy of rheumatoid arthritis, J. Colloid Interface Sci. 544 (2019) 61–77.
[37] V.J. Muniswamy, N. Raval, P. Gondaliya, V. Tambe, K. Kalia, R.K. Tekade, Dendrimer-Cationized-Albumin'encrusted polymeric nanoparticle improves BBB penetration and anticancer activity of doxorubicin, Int. J. Pharm. 555 (2019) 77–99.
[38] R.H.G. Teles, H.F. Moralles, M.R. Cominetti, Global trends in nanomedicine research on triple negative breast cancer: a bibliometric analysis, Int. J. Nanomedicine 13 (2018) 2321.
[39] M. Karakoti, S. Dhali, S. Rana, S.R.V.S. Prasanna, S. Mehta, N.G. Sahoo, Surface **m**odification of **c**arbon-**b**ased Nanomaterials for **p**olymer nanocomposites, Carbon-Based Polymer Nanocomposites for Environmental and Energy Applications, Elsevier, 2018, pp. 27–56.
[40] S. Singh, N.K. Mehra, N. Jain, Development and characterization of the paclitaxel loaded riboflavin and thiamine conjugated carbon nanotubes for cancer treatment, Pharm. Res. 33 (2016) 1769–1781.
[41] J. Wang, W. Ma, Q. Guo, Y. Li, Z. Hu, Z. Zhu, X. Wang, Y. Zhao, X. Chai, P. Tu, The effect of dual-functional hyaluronic acid-vitamin E succinate micelles on targeting delivery of doxorubicin, Int. J. Nanomedicine 11 (2016) 5851.
[42] M. Kumar, G. Sharma, C. Misra, R. Kumar, B. Singh, O. Katare, K. Raza, N-desmethyl tamoxifen and quercetin-loaded multiwalled CNTs: **a** synergistic approach to overcome MDR in cancer cells, Mater. Sci. Eng. C 89 (2018) 274–282.
[43] R. Ansari, R. Gholami, S. Sahmani, A. Norouzzadeh, M. Bazdid-Vahdati, Dynamic stability analysis of embedded multi-walled carbon nanotubes in thermal environment, Acta Mechanica Solida Sinica 28 (2015) 659–667.